

Ellipsoidal Coulomb Crystals in a Linear Radiofrequency Trap

U. Fröhlich, B. Roth, and S. Schiller

Institut für Experimentalphysik, Heinrich-Heine-Universität Düsseldorf, 40225 Düsseldorf, Germany

A static quadrupole potential breaks the cylindrical symmetry of the effective potential of a linear rf trap. For a one-component fluid plasma at low temperature, the resulting equilibrium charge distribution is predicted to be an ellipsoid. We have produced laser-cooled Be^+ ellipsoidal ion crystals and found good agreement between their shapes and the cold fluid prediction. In two-species mixtures, containing Be^+ and sympathetically cooled ions of lower mass, a sufficiently strong static quadrupole potential produces a spatial separation of the species.

One-component plasmas have attracted significant attention in the past, since they represent simple multi-particle systems that can be studied under a variety of conditions with a high degree of experimental control. Detailed theoretical analysis, both analytical and by molecular dynamics (MD) simulations, is possible [1, 2]. To overcome the Coulomb repulsion, the plasmas are confined in Penning- or Paul-type traps. Their temperature can be varied over many orders of magnitude. In particular, they can be efficiently cooled to the mK range by laser cooling. Strong cooling results in phase transitions to a crystalline state, whose occurrence is described by the interaction parameter $\Gamma = Q^2/4\pi\epsilon_0ak_B T$, the ratio between average nearest-neighbor Coulomb energy (a : average particle spacing, Q : particle charge) and thermal energy. MD simulations on infinite systems have shown that the plasma becomes fluid, i.e. exhibits spatial correlations for $\Gamma \geq 2$, without going through a discontinuous gas-fluid phase transition [2]. For $\Gamma > 170$ [3] a phase transition to a crystal occurs. Coulomb crystals in hyperbolic [4] and linear Paul (rf) traps [5, 6] have become of great importance in quantum optics, where they can be used to implement quantum gates or quantum memories [7], and can serve as systems for precision measurements on atomic or molecular ions [8, 9].

The spatial distribution of a trapped one-component gaseous plasma differs significantly from the fluid and crystalline state. This is described by the Debye length $\lambda_D = (k_B T \epsilon_0 / n Q^2)^{1/2}$ which is the distance at which interactions between individual particles overcome collective effects [2]. Here, n is the particle density of the plasma. When λ_D is much larger than the spatial extent of the plasma, the Coulomb interaction is negligible, and the density is a local function of the trap potential only. For a harmonic potential, the density has a Gaussian dependence on the coordinates, with extensions inversely proportional to the respective trap potential curvatures. When λ_D is comparable to or smaller than the spatial extent of the plasma (as is the case for the plasmas presented in this paper), space charge becomes important. The density is then a local function of both trap potential and space charge potential. Since the latter depends on the density distribution over the whole space,

a self-consistent density distribution arises, whose shape exhibits a non-trivial dependence on the trap potential curvatures. For cylindrical symmetry, such plasmas are spheroids (ellipses of revolution) and have been studied both in linear rf and Penning traps [10, 12]. In absence of cylindrical symmetry the shape has been predicted to be that of an ellipsoid [13]. Ellipsoidal plasmas have already been observed and studied in Penning traps (see [14] and references therein). In this work we describe the observation and characterization of cold ellipsoidal plasmas in a linear rf trap. In particular, we have obtained ellipsoidal crystals containing two different ion species.

The linear rf trap used in this experiment consists of four rods of radius r' (inset in Fig.2), each divided into three electrically isolated segments. A radio frequency voltage $V_{RF} \sin \Omega t$ and a static voltage V_{DC} are applied to the rods in a quadrupolar configuration. Confinement along the trap axis (z -axis) is achieved by raising the two end segments of each rod by a static voltage V_{EC} . When the Mathieu stability parameter $q = 2QV_{RF}/mr_0^2\Omega^2 \ll 1$, the independent motion of the trapped ions (mass m) can be adequately described by the motion in an harmonic effective potential (pseudopotential) $U_{trap}(\mathbf{r}) = m \sum \omega_i^2 x_i^2 / 2$ [15], and an additional jitter motion at the radio frequency Ω , the so-called micromotion. r_0 is the minimum distance from the electrode surfaces to the trap axis. The axial (ω_z) and transverse (ω_x and ω_y) frequencies of the effective trap potential are given by $\omega_z^2 = 2\kappa QV_{EC}/m$, $\omega_{x,y}^2 = Q^2 V_{RF}^2 / (2m^2 \Omega^2 r_0^4) - \omega_z^2 / 2 \pm QV_{DC} / mr_0^2$, where κ is a constant determined by the trap geometry. For vanishing static voltage V_{DC} , ω_x and ω_y are degenerate. With the application of a static voltage $V_{DC} \neq 0$, a static quadrupole potential is added to the effective trap potential and the cylindrical symmetry is broken. The transverse trap frequencies ω_x and ω_y increase and decrease, respectively, until ω_y vanishes for a sufficiently large applied voltage V_{DC} , which implies that the ion motion along the y -direction becomes unstable.

In the fluid phase, a trapped plasma in thermal equilibrium at a given temperature T may be regarded as a macroscopic charged fluid with number density $n_f(\mathbf{r})$ [2, 16]. This description leads to an expression for e.g.

the equilibrium shape of the trapped plasma. A particularly simple analytical treatment is possible in the limit of an ultracold plasma, when $T \rightarrow 0$. In this case, the equilibrium number density $n_f(\mathbf{r})$ is determined by the condition of no net force on any plasma region. However, at very low temperatures, the plasma does not remain fluid, but crystallizes with the appearance of shells and a fairly complicate order. While the fluid description may be expected to become inaccurate in this case, it has been shown to remain applicable as far as the shape of the outer boundary is concerned and as long as the crystals are sufficiently large. For linear rf traps, this comparison has so far only been performed for the case of cylindrical symmetry ($V_{DC} = 0$) [10].

In the effective potential approximation, the absence of net force implies a balance between the electric field due to the space charge potential $\phi_f(\mathbf{r})$ and the trap force due to the effective potential: $Q\phi_f(\mathbf{r}) + U_{trap}(\mathbf{r}) = \text{const}$. The number density follows directly from Poisson's equation, $n_f(\mathbf{r}) = (\epsilon_0/Q^2)\Delta U_{trap}(\mathbf{r})$. For the harmonic effective potential of the linear rf trap with the above trap frequencies the number density is explicitly given by $n_0 = \epsilon_0 V_{RF}^2 / m\Omega^2 r_0^4$, which is constant within the fluid and independent of the static voltages V_{DC} and V_{EC} . The outer shape of the zero temperature charged fluid with constant number density is an ellipsoid with principal axes R_x , R_y and L in the x -, y - and z -direction, respectively [13]. With the additional boundary condition that the electric space charge potential $\phi_f(\mathbf{r})$ vanishes at infinity, the potential inside the fluid is given by

$$\phi_f(\mathbf{r}) = \frac{Qn_0}{4\epsilon_0} [A_x(R_x^2 - x^2) + A_y(R_y^2 - y^2) + A_z(L^2 - z^2)], \quad (1)$$

where the dimensionless functions A_x , A_y and A_z depend on the principal axes R_x , R_y and L [13]. Force balance implies that the A_i satisfy $\omega_i^2 = Q^2 n_0 A_i / 2m\epsilon_0$. The ratios of the principal axes R_x/L and R_y/L can thus be calculated by solving the set of equations

$$\begin{aligned} \left(\frac{\omega_x}{\omega_z}\right)^2 &= \frac{A_x(R_x/L, R_y/L)}{A_z(R_x/L, R_y/L)} \\ \left(\frac{\omega_y}{\omega_z}\right)^2 &= \frac{A_y(R_x/L, R_y/L)}{A_z(R_x/L, R_y/L)}. \end{aligned} \quad (2)$$

For $V_{DC} = 0$, ω_x and ω_y are equal, and the equilibrium shape of the zero temperature charged fluid is a spheroid with radius $R := R_x = R_y$ and half length L . The two equations (2) then reduce to a single equation for the aspect ratio R/L . Hornekær et al. [10, 11] have found good agreement between this theory and experimental aspect ratios of a large variety of spheroidal $^{40}\text{Ca}^+$ ion crystals, obtained by varying the end-cap voltage V_{EC} and radio frequency amplitude V_{RF} .

We have tested the predictions of the charged fluid

model in a fully anisotropic effective trap potential using a laser-cooled $^9\text{Be}^+$ ensemble. The linear trap properties were $r_0 = 4.32$ mm, a radio frequency $\Omega/2\pi = 14.2$ MHz with an amplitude $V_{RF} = 380$ V. This resulted in a small Mathieu stability parameter of $q = 0.055$, implying that the micromotion was relatively small and that the effective potential description is appropriate. For axial confinement, $V_{EC} = 4.5$ V was applied to the trap end segments, giving rise to $\kappa = 3.0 \cdot 10^{-3}/\text{mm}^2$, an axial frequency of $\omega_z = 2\pi \cdot 85$ kHz, and a transverse frequency of $\omega_r = 2\pi \cdot 268$ kHz. Experimentally, both values were obtained from a measurement of the transverse frequency as a function of V_{EC} , in absence of V_{DC} . This was done by external excitation of the radial motion of gas phase $^9\text{Be}^+$ ions in the harmonic trap potential, which was detected by a drop of the fluorescence signal from the laser cooled $^9\text{Be}^+$ ions [17].

When the effective trap potential is made anisotropic by application of V_{DC} the predicted instability limit is 4.96 V. We observe partial particle loss when V_{DC} exceeds 4.2 V and total loss at $V_{DC} = 4.9$ V. To prevent particle loss, we limited V_{DC} to a maximum of 4.2 V, corresponding to an increase of the transverse trap frequency $\omega_x/2\pi$ from 268 kHz to 365 kHz and a decrease of $\omega_y/2\pi$ from 268 kHz to 104 kHz. Experimentally, the two transverse frequencies ω_x and ω_y can be measured by secular excitation.

The trap was loaded with $^9\text{Be}^+$ ions by evaporating beryllium atoms from an oven and ionizing them in the trap center by electron impact. The trapped $^9\text{Be}^+$ ions, initially forming a hot plasma cloud of ≈ 1000 K, were laser cooled by laser radiation at 313 nm until they finally underwent a phase transition to a crystalline state with a temperature of a few mK. A description of the all-solid-state laser system is given in [18]. To image the $^9\text{Be}^+$ ion crystals, a CCD camera was placed transverse to the trap axis. Fig.1 shows an ion crystal containing $\simeq 2.0 \times 10^3$ $^9\text{Be}^+$, at different values of V_{DC} . The estimate of the ion number in Fig.1 (a) is obtained from molecular dynamics (MD) simulations in which the observed structure (especially the number of shells) is reproduced [19]. For the test of the calibration of the CCD optics magnification as well as the determination of absolute dimensions of the ion plasmas, we also use the MD simulations. As a check, multiplying the volume $4\pi R_{45}^2 L/3$ of the crystal shown in Fig.1 (a) and the cold fluid model density n_0 , we obtain the value $\simeq 2.0 \times 10^3$. This agrees well with the MD results and implies that the model is applicable for large crystals.

In the outer region of the crystal shown in Fig.1 the ions are arranged in concentric shells, while the core appears to be fluid. The size of the liquid core appears to increase with applied static quadrupole potential. A possible explanation for this behavior is the increased thermal motion of the ions in the core, which was reproduced by MD simulations and is a subject of ongoing studies.

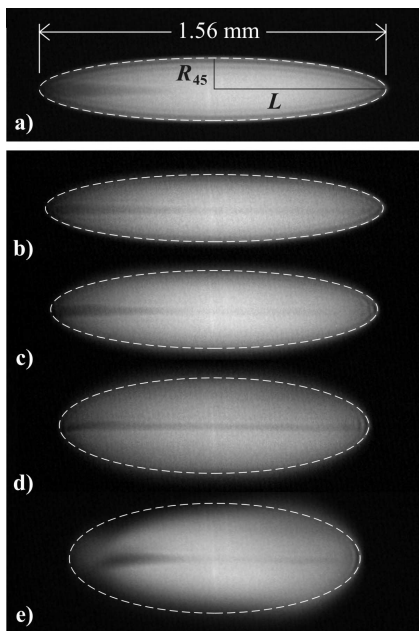


FIG. 1: CCD images of a large ion crystal containing $\simeq 2.0 \times 10^3$ ${}^9\text{Be}^+$, taken perpendicular to the z -axis and at 45° to the x - and y -axes, for different values of V_{DC} . Dashed lines: fits of ellipses with principal axes R_{45} and L to the outermost shells. (a): $V_{DC} = 0$, the effective trap potential has cylindrical symmetry. The ion crystal is a prolate spheroid with radius $R_x = R_y = R_{45}$ and half length L . The aspect ratio $R_{45}/L = 0.178$. (b)-(e): $V_{DC} \neq 0$, the cylindrical symmetry is broken and the crystal is an ellipsoid with principal axes $R_x < R_{45}$, $R_y > R_{45}$ and L . With increasing V_{DC} the crystal expands in the y -direction and compresses in the x - and z -directions, while maintaining constant volume. V_{DC} is set to 1.8 (b), 2.8 (c), 3.6 (d) and 4.2 V (e), leading to an aspect ratio of $R_{45}/L = 0.193$ (b), 0.235 (c), 0.309 (d), and 0.413 (e). For a definition of R_x , R_y and R_{45} see inset of Fig.2.

In contrast to the observation of partially crystallized large plasmas, we found that under similar laser cooling parameters small plasmas containing only a few hundred ${}^9\text{Be}^+$ ions always crystallized completely. The left central part of the ion crystal contains a dark region, which consists of sympathetically cooled ions originating from the residual gas and having a mass smaller than that of ${}^9\text{Be}^+$, pushed to one side by radiation pressure [20].

The ellipsoidal deformation is a reversible process if the maximum value of V_{DC} is kept within the range stated above: after turning V_{DC} off, the principal axes R_{45} and L of the crystal returned to the initial values, indicating that no ions were lost during deformation. The outer boundaries of the crystals in Fig.1 can be well described by ellipses with principal axes R_{45} and L . Since the CCD camera takes a projection along an axis at 45° with respect to the x - and y -axes, the principal axis R_{45} of each ellipse is related to the principal axes R_x and R_y of the corresponding ellipsoid by $R_{45} = [(R_x^2 + R_y^2)/2]^{1/2}$.

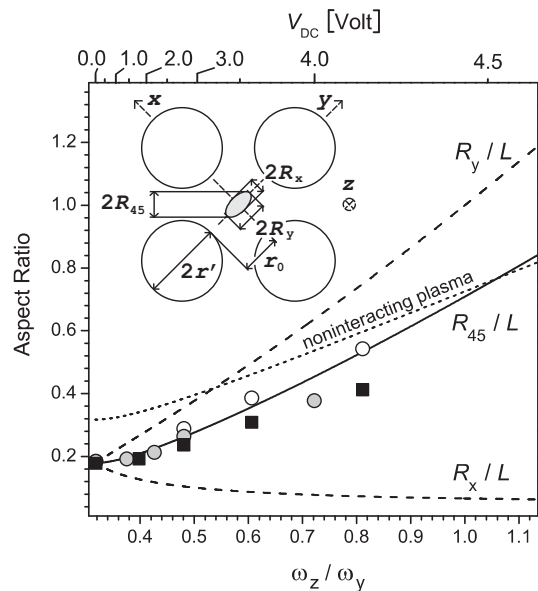


FIG. 2: Comparison of the aspect ratio R_{45}/L of a partially crystallized ${}^9\text{Be}^+$ plasma and the cold fluid prediction for zero-temperature ellipsoidal plasmas, as a function of the ratio ω_z/ω_y between the axial and the smallest transverse trap frequency. Full squares: large crystals from Fig.1. Open (gray) circles: small (medium-size) crystals from Fig.3. Dotted line: R_{45}/L for a low-density plasma in the gas phase with negligible particle interactions, leading to $R_x/L = \omega_z/\omega_x$, $R_y/L = \omega_z/\omega_y$. Inset: Cross-section of linear trap and of ellipsoidal plasma. Observation direction as in Fig.1.

For the last crystal in the sequence, the boundary shows clear deviations from an ellipse; we attribute this to the presence of sympathetically cooled impurities of higher mass than ${}^9\text{Be}^+$, located at larger radii as compared to ${}^9\text{Be}^+$. The asymmetry along the trap axis is caused by cooling light pressure, which is not felt by the sympathetically cooled ions. In this case, the elliptical fit has been chosen to match the fragments of the outermost shell, which still exist at the left and right ends of the crystal.

Fig.2 shows a comparison between the measured aspect ratio R_{45}/L and the theoretical result from Eq.(2). The agreement between experiment and theory is good, considering that the ${}^9\text{Be}^+$ ion crystals did exhibit two phases and were not pure. In addition, a systematic deviation between theory and experiment is expected at the largest applied voltages V_{DC} because then the smallest ellipsoid dimension, R_x , becomes comparable to the shell spacing. In this limit, the cold fluid model continuum description is inaccurate.

The cold fluid model also determines the relative change of the crystal length $2L$ when V_{DC} is changed. For the actual trap settings $2L$ is expected to decrease to 83% from its initial value, when changing V_{DC} from 0 to 4.2 V. The length of the crystal in the last image (e) in Fig.1 is 84% of the initial one (a), in good agreement

with the expected compression. Therefore, while at large V_{DC} the observed transverse crystal shape starts to deviate from the predictions of the cold fluid model, the axial shape is still in good agreement, since the axial dimension of the crystal remains large compared to the shell spacing.

While for large Coulomb crystals a spatially averaged description is a good first approximation, in small crystals one may expect effects related to the particle structure to show up clearly. As an example, Fig.3 (a)-(d) shows a crystal containing about 20 ${}^9\text{Be}^+$ ions and several sympathetically cooled low-mass impurities. In an effective trap potential with cylindrical symmetry, the crystal exhibits a single ${}^9\text{Be}^+$ shell, Fig.3 (a). This shell appears smeared out in the CCD image (exposure time: 2 s), possibly because of a rotation-like diffusion of the ions around the trap axis. In the ellipsoidal crystals, Fig.3(b)-(d), this diffusion is suppressed because it would require overcoming an energy barrier, and therefore the image shows individual ions. The most apparent property arising when the static voltage V_{DC} is increased is the completely dark region containing the sympathetically cooled particles. Furthermore, some of the fluorescence spots representing ${}^9\text{Be}^+$ ions appear smeared out and show a reduced intensity. We attribute this to the micromotion occurring at the locations of these ions. As a test, we shifted the crystal by means of an additional static voltage applied to one trap electrode. This caused a rearrangement of the ${}^9\text{Be}^+$ relative to the dark core, but those ions that appeared well defined were always in the same region. Although the small crystal (a)-(d) in Fig.3 does not exhibit closed boundaries, we could still fit ellipses to them. In order to compare such small crystals with the cold fluid model, half of the typical shell spacing of $29\ \mu\text{m}$ was added to R_{45} and L before calculating the ratio R_{45}/L . The results are indicated by open circles in Fig.2. Even for this case there is a good agreement with the cold fluid model. Finally, in Fig.3 (e)-(h) we also present a medium-sized crystal containing $\simeq 500$ ${}^9\text{Be}^+$ ions and, again, additional low-mass impurities. The corresponding aspect ratio data as well as an additional data point for $V_{DC} = 2.2\ \text{V}$, reported in Fig.2, also show good agreement with theory. However, for large and medium-sized crystals a deviation between theory and experiment becomes obvious as the values for the static voltage V_{DC} increase. Our molecular dynamics simulations show, that the observed deviations can be explained by small ($< 15\%$) admixtures of sympathetically cooled molecular impurities, in particular, $\text{H}_2^+/\text{H}_3^+$ ions close to the trap axis originating from residual gas contaminants, and BeH^+ ions located in the outer regions of the crystals formed by chemical reactions.

The pronounced asymmetric ion distribution in the small, Fig.3 (a)-(d), as well as in the medium-sized crystal, Fig.3 (e)-(h), is not due to the broken cylindrical

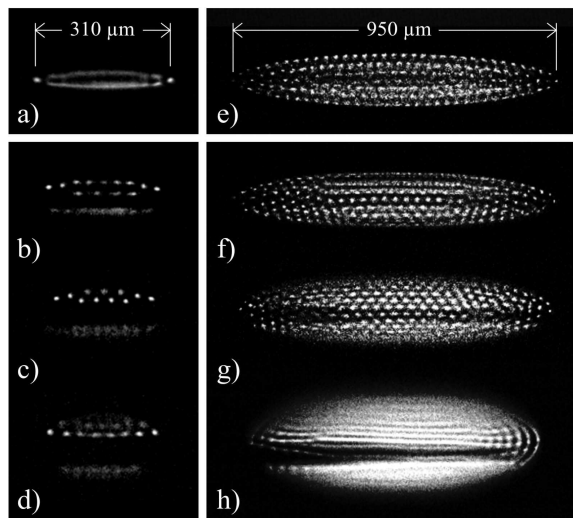


FIG. 3: Left: small crystal containing $\simeq 20$ ${}^9\text{Be}^+$ ions and a smaller number of sympathetically cooled impurity ions at different values of the static voltage V_{DC} : 0 V (a), 2.8 V (b), 3.6 V (c), and 4.2 V (d). Right: medium-size crystal containing $\simeq 500$ ${}^9\text{Be}^+$ ions. V_{DC} is set to 0 V (a), 1.4 V (b), 2.8 V (c), and 4.0 V (d). The asymmetric ion distribution in (b)-(d) and (f)-(h) is due to stray electric fields.

symmetry of the trap potential, as this does not produce any visible asymmetry in the CCD images. Instead, we attribute the asymmetric ion distribution to stray potentials. While it was not possible to compensate for these imperfections by additional static voltages, it was always possible to reverse the asymmetry by means of these voltages. Our MD simulations confirm this interpretation.

A direct estimate for the translational temperature of the Be^+ is obtained from the spectral line shape of its fluorescence as the cooling laser is tuned towards resonance and the ion ensemble crystallizes. Since the temperature of the particles changes during the frequency scan, we fit a Voigt profile to each point of the recorded fluorescence curve to determine an upper limit for the Be^+ temperature. For small crystals (< 1000 particles), we find an upper limit for the temperature at the end of the scan of 42 mK. However, the accuracy of this method is limited due to the experimental resolution. An indirect upper limit is obtained by comparing the size of the ion spots with MD simulations; here we find a tighter limit of < 10 mK for the Be^+ temperature. We deduce, assuming thermal equilibrium, that the temperature of the sympathetically cooled impurity ions in Fig.3 is < 10 mK.

In summary, we have studied the static behavior of Coulomb crystals in a fully anisotropic effective trap potential. We have found a good agreement with the simple cold fluid plasma model for small anisotropy. For larger anisotropy, deviations could be explained by the presence of additional, sympathetically cooled,

ion species. From an experimental point of view, the ability to reversibly deform a crystal permits to separate lower-mass sympathetically cooled ions from the laser-cooled ions. This allows to obtain a clearer picture of the impurity ion ensemble, without any background or foreground fluorescence from laser-cooled ions. This will also permit to manipulate the sympathetically cooled ions in a more direct way. The ability to generate a variety of ellipsoidal crystals opens up several directions for further study, e.g. oscillation modes of such crystals, and in particular the modes of two-species crystals. These modes could be of importance for identification of the non-fluorescent species. On the theoretical side, it is of interest to perform detailed studies of structures using MD simulations, which are able to take fully into account the particle nature of the cold plasmas. As an example, our MD simulations have shown that in strongly squeezed ellipsoids closed ion rings can occur. These represent a novel form of low-dimensional artificial structure whose detailed investigation should be of significant interest.

We thank H. Wenz for the MD simulations. This work was supported by the Deutsche Forschungsgemeinschaft and the EU Network "Ultracold Molecules".

- [2] D.H.E. Dubin and T.M. O'Neil, *Rev. Mod. Phys.* **71**, 87 (1999).
- [3] W.L. Slattey, G.D. Doolen, and H.E. DeWitt, *Phys. Rev. A* **21**, 2087 (1980).
- [4] F. Diedrich et al., *Phys. Rev. Lett.* **59**, 2931 (1987).
- [5] M.G. Raizen et al., *J. Mod. Opt.* **39**, 233 (1992).
- [6] M. Drewsen et al., *Phys. Rev. Lett.* **81**, 2878 (1998).
- [7] M.D. Lukin, S.F. Yelin, and M. Fleischhauer, *Phys. Rev. Lett.* **84**, 4232 (2000).
- [8] D.J. Berkeland et al., *Phys. Rev. Lett.* **80**, 2089 (1998).
- [9] S. Schiller and C. Lämmerzahl, *Phys. Rev. A* **68**, 053406 (2003), S. Schiller and V. I. Korobov, submitted to *Phys. Rev. A*.
- [10] L. Hornekær et al., *Phys. Rev. Lett.* **86**, 1994 (2001).
- [11] L. Hornekær, PhD thesis, Aarhus Univ. (2000).
- [12] L.R. Brewer et al., *Phys. Rev. A* **38**, 859 (1988).
- [13] D. H. E. Dubin, *Phys. Fluids B* **5**, 295 (1992).
- [14] X.-P. Huang, *Phys. Plasmas* **5**, 1656 (1998).
- [15] H. G. Dehmelt, *Adv. At. Mol. Phys.* **3**, 53 (1967).
- [16] L. Turner, *Phys. Fluids* **30**, 3196 (1987).
- [17] T. Baba and I. Waki, *Jpn. J. Appl. Phys.* **35**, L 1134 (1996).
- [18] H. Schnitzler et al., *Appl. Optics*, **41**, 7000 (2002).
- [19] H. Wenz, private communication.
- [20] B. Roth, U. Fröhlich, and S. Schiller, submitted.

[1] R.C. Davidson, *Physics of Nonneutral Plasmas*, (Imperial College Press, 2001).